

Article

# An Analytical Model to Predict the Effects of Suspended Solids in Injected Water on the Oil Displacement Efficiency during Waterflooding

Slavko Nestic <sup>1,\*</sup>, Anatoly Zolotukhin <sup>2</sup>, Vladimir Mitrovic <sup>1</sup>, Dragan Govedarica <sup>3</sup> and Afshin Davarpanah <sup>4</sup>

<sup>1</sup> Faculty of Mining and Geology, University of Belgrade, 11000 Belgrade, Serbia; vlada.nafta@gmail.com

<sup>2</sup> Gubkin Russian State University of Oil and Gas (National Research University), 119991 Moscow, Russia; anatoly.zolotukhin@gmail.com

<sup>3</sup> Faculty of Technology, University of Novi Sad, 21000 Novi Sad, Serbia; dragang@uns.ac.rs

<sup>4</sup> Department of Mathematics, Aberystwyth University, Aberystwyth SY23 3BZ, UK; afd6@aber.ac.uk

\* Correspondence: slavko.nestic@nis.eu or slavkonesic@yahoo.com; Tel.: +381-64-4384244

Received: 7 May 2020; Accepted: 30 May 2020; Published: 2 June 2020



**Abstract:** Suspended solids in the injection water cause impairment of water injectivity during waterflooding operations. Suspended solids affect reservoir properties and decrease the permeability of reservoir rocks causing an increase of injection pressure and a decrease in water injectivity. Removal of all suspended solids from injection water is an expensive and economically unfeasible process. To minimize the effects of suspended solids to the formation, it is necessary to determine an impairment mechanism of suspended solids on oil displacement and, therefore, optimize the water treatment process. In this paper, an analytical model that describes the relationship between injection water quality and impairment mechanisms on oil displacement is presented. A formation impairment was calculated, introducing the parameter called impairment ratio, which represents the ratio between suspended solids and pore size distribution of reservoir rock. Based on the impairment ratio, decreases in porosity and permeability were calculated with changes in capillary pressure, relative permeability, and displacement efficiency. The model was tested for three different types of injection water. Results indicated the presence of formation impairment even with the smallest particles. Suspended solids had the greatest influence on porosity and permeability impairment. The model could be used as input for reservoir modelling studies for monitoring and controlling displacement efficiency during waterflooding as well as for planning and modification of water treatment units.

**Keywords:** waterflooding; formation damage; suspended solids; oil displacement

## 1. Introduction

Waterflooding methods in hydrocarbon reservoirs are known as widely common methods used to enhance oil recovery by maintaining reservoir pressure and increasing oil displacement efficiency toward production wells. They are some of most efficient methods for increasing oil recovery as confirmed in numerous studies and oilfields [1,2]. The injected water used in waterflooding operations is usually oilfield produced water, freshwater, or seawater, depending on the geographical location and availability. Injection of treated produced water is highly recommended for waterflooding operations. Oilfield produced water is a toxic waste and requires proper waste management to minimize the environmental impact. Reusing produced water decreases the cost of water disposal and reduces environmental pollution risks [3,4]. Statistically, around 20% of waterflooding projects do not reach planned effects due to the injected water quality and associated formation damage that causes reduction

of formation permeability and injectivity [5]. Impairment of permeability was observed in many laboratory experiments and is associated with the plugging of pore space with suspended solids in injection water [6–9]. Suspended solids in injection water originate from silts, clays, different types of scales, products of bacterial activity, or erosion of rock during oil production. Along with formation impairment, fines migration causes changes in relative permeability and affects oil displacement [10]. To avoid those problems with injectivity, water needs to be adequately treated before injection to minimize formation damage and require additional costs. Otherwise, water injectivity can be enhanced with stimulation of injection wells with acid treatment [11–13]. During waterflooding, when injection water that contains suspended solids enters into a porous media, smaller solids will flow through the pore system and form an internal filter cake, while larger particles will deposit on the surface and form an external filter cake. Both internal and external filter cakes affect water injectivity and cause an increase in injection pressure [7,14–16]. Pore size distribution (PSD) is one of the parameters governing reservoir performance during the waterflooding process. It is a critical parameter for oil displacement efficiency by influencing porosity, permeability, and residual oil saturation [16]. It is essential to study the pore structure of reservoir rocks for a better understanding of fluid flow through porous media and displacement efficiency. Reservoir performance during a waterflooding operation is dependent on rock-typing and PSD and suspended solids distribution (SSD) in injected water. In this study, the effects of suspended solids on the waterflooding process were analyzed based on PSD and SSD. The effects on formation parameters, oil displacement, and a new model are also presented.

## 2. Literature Review

Impairment of well injectivity, due to the presence of suspended solids in injection water, is thoroughly described and many analytical models for injectivity prediction have been developed. Gruesbeck and Collins developed the theory of fines deposition and entrainment in porous media. In their study, the influence of naturally occurring particles to productivity decline in producing wells was confirmed with experimental results. With different flow rate variations, they observed a critical flow velocity in which entrainment of naturally occurred solid particles becomes essential [17]. Barkman and Davidson introduced the water quality ratio (WQR), which was obtained from filter tests and core data analysis for prediction of formation impairment by suspended solids. They modelled four mechanisms of formation impairment for constant pressure drop conditions and they can be applied to the planning and optimization of produced water treatment projects [6]. Tod et al. investigated the effects of suspended solids on permeability and injectivity decline on a reservoir core sample. The results showed that the formation damage with the suspension of particles was less than 3  $\mu\text{m}$ . Similar results were found with large particles (4–6  $\mu\text{m}$ ), whereas larger particles (8–10  $\mu\text{m}$ ) formed external filter cake [18]. By using an electrical analogy theory to simulate flow resistance, Khatib introduced a new model for the calculation of the matrix and filter cake resistance in perforations and fractures. The results showed that the type of suspended solids had significant effects on the buildup of the filter cake, and the properties of a formed filter cake varied with changes in pressure [13]. Shutong and Sharma used the transition time concept to model injectivity decline considering the buildup of internal and external filter cake. They obtained good results but required core data [14]. Davidson studied the effects of flow velocity and particle invasion through the formation and developed a correlation between core data and particle invasion [19]. Vitthal et al. presented a network model to simulate the impairment of permeability due to fines migration or injection in radial geometry. Their results showed that impairment is more severe in radial flow geometry compared with linear flow and the concentration of fines is higher in the invading front [20]. Oort et al. developed a new model for the formation impairment during waterflooding by internal filter cake where formation damage was expressed semi-empirically. Their results indicated that the impairment rate strongly depends on flow velocity at the injection surface. Formation impairment decreases with increasing flow velocity and it is susceptible to changes in velocity [21].

### 3. Materials and Methods

The presented model requires a comprehensive reservoir characterization. Before the implementation of the presented model, the following lab tests should be conducted on core samples to define reservoir properties and water analysis to obtain the following parameters:

- Porosity and pore size distribution (particle size analysis (PSA), nuclear magnetic resonance (NMR))
- Reservoir permeability (permeability tests on core samples)
- Distribution of suspended solids in injected water (PSA)
- Capillary pressure (lab)

Data accuracy must be high and a large number of core samples are recommended due to the accuracy of measurements, especially in the analysis of porosity and pore size distribution due to its influence on the analysis. Permeability tests should be conducted on core samples in every part of the reservoir, especially in more heterogeneous layers. Particle size analysis is a dynamic parameter that needs to be measured periodically. For capillary pressure, lab tests are recommended [22]. The simplified workflow of the model is shown in Figure 1.

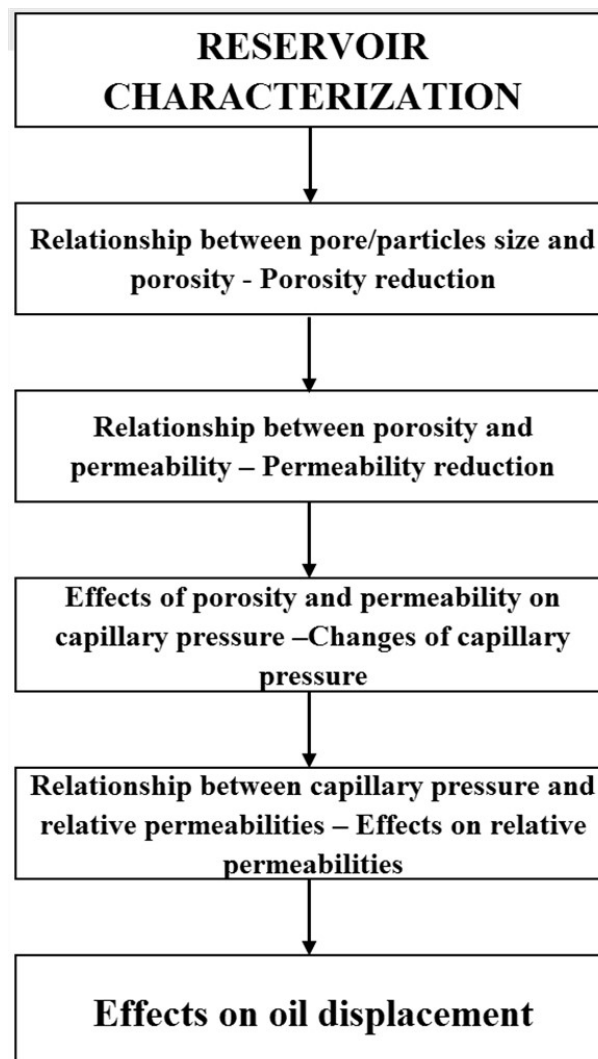


Figure 1. The simplified workflow of the model.

An analytical model for predicting the effects of suspended solids in injection water on oil displacement during waterflooding can be calculated through the following 5 steps:

**Step 1.** From the pore size distribution of a reservoir core sample and suspended solids size distribution in injected water, determine the changes in porosity.

**Step 2.** Determine permeability reduction from the porosity/permeability relationship.

**Step 3.** From Leverett  $J$  function ( $S_w$ ) for changed values of porosity ( $\phi$ ) and permeability ( $K$ ), determine a change in capillary pressure ( $P_c$ ).

**Step 4.** From capillary pressure data, calculate relative permeabilities for oil and water using the modified Brooks and Corey correlations.

**Step 5.** Calculate the Buckley–Leverett curve for oil displacement. The model has several assumptions and constraints, including:

- Fluid–rock interaction is neglected;
- Compatibility of injected and reservoir water is neglected, i.e., waters are compatible
- Mechanism of suspended solids deposition is sedimentation; and
- Particle erosion during waterflooding is neglected.

### 3.1. Relationship between Pore/Particle Size and Porosity—Porosity Reduction Model

Pores in the reservoir rock are spaces for storage of reservoir fluids. Variations in pore size and pore geometry lead to the reservoir heterogeneity. Pore size distribution is an essential factor for the planning of waterflooding projects because of sweep efficiency. Characterization of pore size distribution was studied in many articles [23–38]. Methods for the determination of porosity and pore size distributions are shown in Figure 2 [39], namely: atomic force microscopy (AFM), small angle neutron scattering (SANS), ultra-small angle neutron scattering (USANS), small-angle X-ray scattering (SAX), and Brunauer, Emmett, and Teller gas adsorption method (BET).

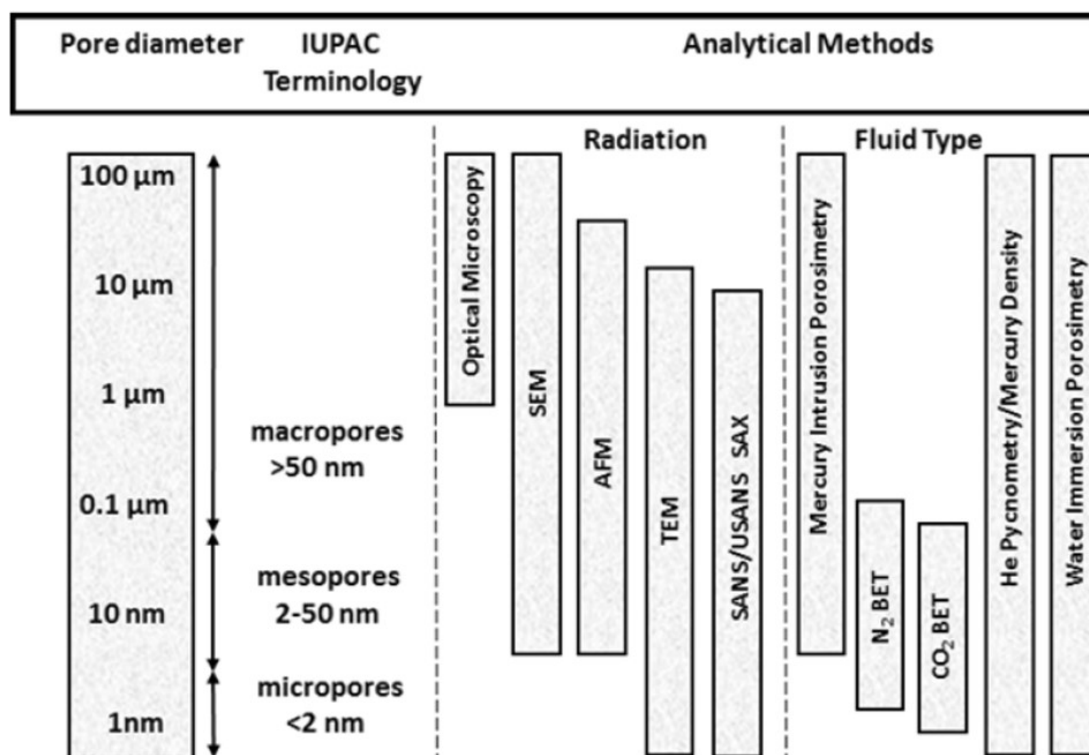


Figure 2. Methods used for measurements of porosity and pore size distribution.

For this model, suspended solids/pore size distribution is classified in 10 different classes according to the defined diameter ranges.

The term *impairment ratio (IR)* is introduced, describing the ratio between the distribution of suspended solids and pore size distribution:

$$IR = \frac{d_{ssi}}{d_{psi}} \quad (1)$$

where  $d_{ssi}$  is the pore size distribution of suspended solid and  $d_{psi}$  is the pore size distribution. Classification of suspended solids/pore size with impairment ratio is shown in Table 1.

**Table 1.** Classification of suspended solids/pore size with impairment ratio.

Class	1	2	3	4	5	6	7	8	9	10
Diameter range ( $\mu\text{m}$ )	0–5	5–10	10–15	15–20	20–30	30–50	50–70	70–100	100–150	150+
Pore size distribution (%)	$d_{ps1}$	$d_{ps2}$	$d_{ps3}$	$d_{ps4}$	$d_{ps5}$	$d_{ps6}$	$d_{ps7}$	$d_{ps8}$	$d_{ps9}$	$d_{ps10}$
Suspended solids distribution (%)	$d_{ss1}$	$d_{ss2}$	$d_{ss3}$	$d_{ss4}$	$d_{ss5}$	$d_{ss6}$	$d_{ss7}$	$d_{ss8}$	$d_{ss9}$	$d_{ss10}$
Impairment ratio (IR)	$d_{ss1}/d_{ps1}$	$d_{ss2}/d_{ps2}$	$d_{ss3}/d_{ps3}$	$d_{ss4}/d_{ps4}$	$d_{ss5}/d_{ps5}$	$d_{ss6}/d_{ps6}$	$d_{ss7}/d_{ps7}$	$d_{ss8}/d_{ps8}$	$d_{ss9}/d_{ps9}$	$d_{ss10}/d_{ps10}$

Fractional porosity can be expressed from the percentage of pore space and total porosity. Porosity can be expressed as a sum of fractional porosities for every pore diameter range:

$$\Phi = \sum_{n=1}^{10} \Phi_n \quad (2)$$

where  $\phi_1$ – $\phi_{10}$  are fractional porosities from class 1 pores to class 10 pores. Porosity decrease is based on the suspended solids/pore size ratio and can be calculated using the following rules:

- If the ratio between the suspended solids fraction and pore diameter is between 0.0 and 0.7, there will be no changes in fractional porosity.
- If the ratio between the suspended solids fraction and pore diameter is between 0.7 and 1, fractional porosity for specific diameter will be multiplied by 0.8.
- If the ratio between the suspended solids fraction and pore diameter is between 1 and 2, fractional porosity for specific diameter will be multiplied by 0.6.
- If the ratio between the suspended solids fraction and pore diameter is higher than 2, fractional porosity for specific diameter will be multiplied by 0.5.

### 3.2. Relationship between Porosity and Permeability—Permeability Reduction Model

The relationship between porosity and permeability is significant and fundamental for many reservoir engineering studies. Studies about the relationship between porosity and permeability date back to the 20th century. Many scientists attempted to find a definite and predictable correlation [40,41]. Reservoir permeability can be expressed as a function of porosity but many factors, including pore size arrangement and distribution, contribute to their relationship. One of the most uncomplicated porosity–permeability relationships was presented by the Kozeny–Carman equation [42]:

$$K = C \cdot \frac{\phi}{S_p^2} \quad (3)$$

where  $S_p$  is surface area per unit of pore volume and  $C$  is constant depending on the cementation degree. Kotyakhov suggested a relationship between porosity and permeability as follows [43]:

$$K = \frac{d_e \cdot \phi^3}{72 \cdot (1 - \phi)^2} \quad (4)$$

where  $d_e$  is the effective grain diameter.

Relationship between porosity and permeability can be expressed as a power-law correlation [44]:

$$K \approx \phi^n \quad (5)$$

The porosity–permeability relationship in limestone varies in a range of several orders of magnitude. Permeability depends on pore space, which is characterized by the porosity and pore size distribution in a rock sample [45,46]. In many sandstone and carbonate reservoir rocks, plotting porosity vs. logarithm of permeability is often a linear function. The slope of the line is a function of many factors, including grain size and sorting, and diagenetic and compaction history. For unconsolidated formations, better grain sorting will increase both porosity and permeability. The increase of grain size will increase permeability even with decreased porosity. The presence of clays, cement, and diagenetic minerals tends to decrease permeability as porosity decreases [47].

### 3.3. Effects of Porosity and Permeability on Capillary Pressure—Changes of Capillary Pressure

The capillary pressure data  $J(S_w)$  function can be calculated as follows [48]:

$$J(S_w) = \frac{P_c(S_w)}{\sigma \cdot \cos \theta} \cdot \sqrt{\frac{K}{\phi}} \quad (6)$$

where  $S_w$  is water saturation,  $\sigma$  is surface tension, and  $\theta$  is contact angle. The square root of permeability over porosity is known as rock quality index (RQI) [49]. Then, the equation can be rewritten:

$$J(S_w) = \frac{P_c(S_w)}{\sigma \cdot \cos \theta} \cdot RQI \quad (7)$$

Changes in capillary pressure can be recalculated for every change of  $K$  and  $\phi$ :

$$P_c(S_w) = \frac{J(S_w) \cdot \sigma \cdot \cos \theta}{RQI} \quad (8)$$

### 3.4. Relationship between Capillary Pressure and Relative Permeabilities—Effects on Relative Permeabilities

Relative permeability can be calculated from capillary pressure data using Brooks and Corey correlations [50]:

$$K_{rw} = (S_w^*)^{\frac{2+3\lambda}{\lambda}} \quad (9)$$

$$K_{ro} = (1 - S_w^*)^2 \cdot \left[ (1 - S_w^*)^{\frac{2+3\lambda}{\lambda}} \right] \quad (10)$$

where  $S_w^*$  is effective water saturation and  $\lambda$  is pore size distribution index. Here, the rock quality index (RQI) is used to describe changes in relative permeability. The relationship between original and changed permeability and porosity is described introducing the rock quality index ratio ( $R_{RQI}$ ):

$$R_{RQI} = \frac{RQI}{RQI'} \quad (11)$$

where  $RQI$  is initial rock quality index ratio and  $RQI'$  is rock quality index for reservoir rock affected by suspended solids.

A modification of the Brooks and Corey relative permeability correlation is made by multiplying  $\lambda$  with the rock quality index ratio to express formation impairment:

$$K_{rw} = (S_w^*)^{\frac{2+3\lambda \cdot R_{RQI}}{\lambda \cdot R_{RQI}}} \quad (12)$$

$$K_{ro} = (1 - S_w^*)^2 \cdot \left[ (1 - S_w^*)^{\frac{2+3\lambda \cdot R_{ROI}}{\lambda \cdot R_{ROI}}} \right] \quad (13)$$

### 3.5. Effects on Oil Displacement

From the relative permeability data, the Buckley–Leverett curve can be constructed as follows [51]:

$$f_w = \frac{1}{1 + \frac{K_{ro}}{K_{rw}} \cdot \frac{\mu_w}{\mu_o}} \quad (14)$$

where  $\mu_w$  and  $\mu_o$  are viscosities of water and oil, respectively.

## 4. Results

### 4.1. Porosity Reduction

Pore size distribution is determined from laboratory analysis on core samples from oilfield marked K in Serbia. Three different cases were analyzed with different suspended solids distributions in the injection water: Case I, where injection water contains small-range diameters of suspended solids; Case II, where injection water contains mid-range diameters of suspended solids; and Case III, where injection water contains high-range diameters of suspended solids. The comparison of suspended solids distribution and pore size distribution is shown in Figure 3.



**Figure 3.** Comparison of suspended solids distribution and pore size distribution.

Porosity reduction based on  $IR$  for all three cases is shown in Table 2.

**Table 2.** Porosity reduction based on impairment ratio (IR) for all three cases.

Class	Diameter Range ( $\mu\text{m}$ )	Reservoir		Case I			Case II			Case III		
		Pore Size Distribution (%)	Fractional Porosity	Suspended Solids Distribution (%)	IR	Porosity Decrease	Suspended Solids Distribution (%)	IR	Porosity Decrease	Suspended Solids Distribution (%)	IR	Porosity Decrease
1	0–5	2	0.374	5	2.50	0.187	1	0.50	0.374	1	0.50	0.374
2	5–10	5	0.935	12	2.40	0.468	3	0.60	0.935	2	0.40	0.935
3	10–15	12	2.244	22	1.83	1.346	6	0.50	2.244	2	0.17	2.244
4	15–20	8	1.496	21	2.63	0.748	17	2.13	0.748	3	0.38	1.496
5	20–30	7	1.309	17	2.43	0.655	22	3.14	0.655	3	0.43	1.309
6	30–50	12	2.244	8	0.67	2.244	19	1.58	1.346	4	0.33	2.244
7	50–70	13	2.431	6	0.46	2.431	16	1.23	1.459	16	1.23	1.459
8	70–100	8	1.496	4	0.50	1.496	12	1.50	0.898	22	2.75	0.748
9	100–150	16	2.992	4	0.25	2.992	3	0.19	2.992	26	1.63	1.795
10	150+	17	3.179	1	0.06	3.179	1	0.06	3.179	21	1.24	1.907
	<b>Total</b>	<b>100</b>	<b>18.7</b>	<b>100</b>		<b>15.75</b>	<b>100</b>		<b>14.83</b>	<b>100</b>		<b>14.52</b>

The total porosity of the reservoir is expressed as a sum of fractional porosities:

$$\phi = 0.374 + 0.935 + 2.244 + 1.496 + 1.309 + 2.244 + 2.431 + 1.496 + 2.992 + 3.179 = 18.7\%$$

Based on the calculated IE, porosity decrease calculation for Case I is:

$$\phi = 0.374 \cdot 0.5 + 0.935 \cdot 0.5 + 2.244 \cdot 0.6 + 1.496 \cdot 0.5 + 1.309 \cdot 0.5 + 2.244 \cdot 1 + 2.431 \cdot 1 + 1.496 \cdot 1 + 2.992 \cdot 1 + 3.179 \cdot 1 = 15.75\%$$

Based on the calculated Impairment Ratio, porosity decrease calculation for Case II is:

$$\phi = 0.374 \cdot 1 + 0.935 \cdot 1 + 2.244 \cdot 1 + 1.496 \cdot 0.5 + 1.309 \cdot 0.5 + 2.244 \cdot 0.6 + 2.431 \cdot 0.6 + 1.496 \cdot 0.6 + 2.992 \cdot 1 + 3.179 \cdot 1 = 14.83\%$$

Based on the calculated Impairment Ratio, porosity decrease calculation for Case III is:

$$\phi = 0.374 \cdot 1 + 0.935 \cdot 1 + 2.244 \cdot 1 + 1.496 \cdot 1 + 1.309 \cdot 1 + 2.244 \cdot 1 + 2.431 \cdot 0.6 + 1.496 \cdot 0.5 + 2.992 \cdot 0.6 + 3.179 \cdot 0.6 = 14.51\%$$

#### 4.2. Permeability Reduction

Permeability reduction is determined from the porosity–permeability relationships. Lab tests for porosity and permeability were conducted on 70 core samples from oilfield K in Serbia. The porosity–permeability relationship is shown in Figure 4.

$$K = 2.7 \cdot 10^{-4} \cdot \phi^{4.7878551024} \quad (15)$$

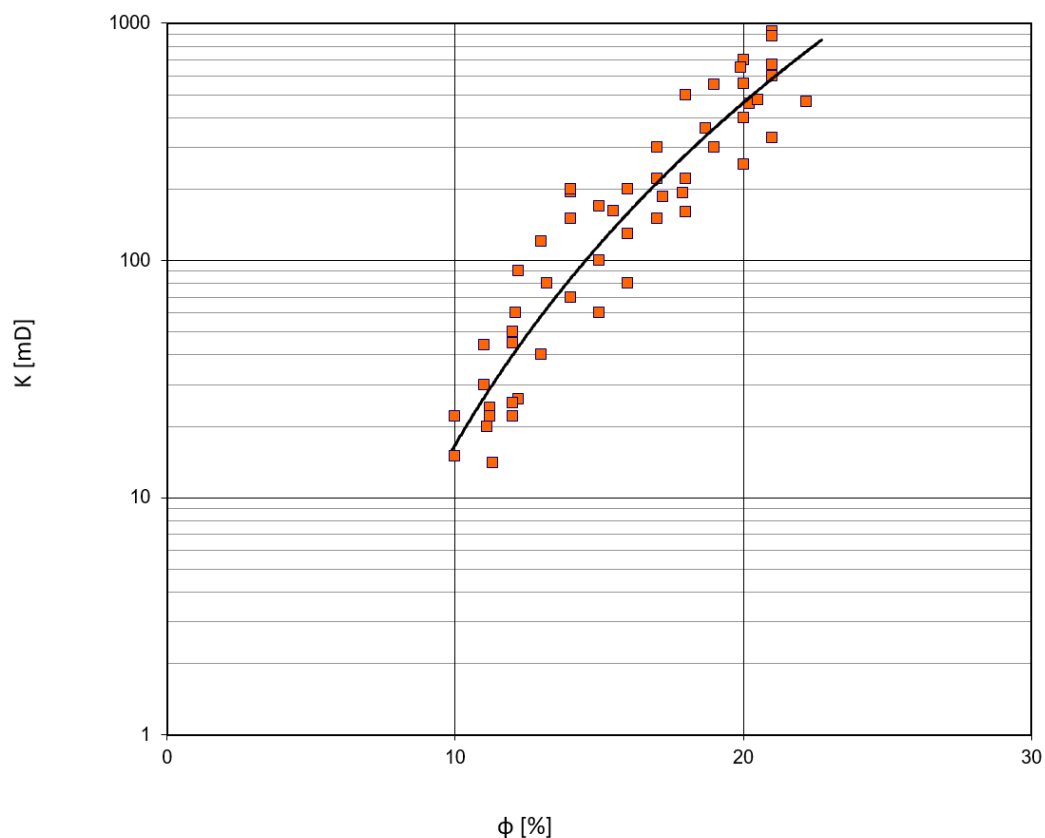


**Figure 4.** Porosity–permeability relationship.

Changes in porosity and permeability for all three cases are shown in Table 3.

**Table 3.** Changes in porosity ( $\phi$ ) and permeability ( $K$ ) for all three cases.

	Reservoir	Case I	Case II	Case III
$\phi$	18.70	15.75	14.83	14.51
$K$	335.32	147.19	110.46	99.57

#### 4.3. Changes in Capillary Pressure

Capillary pressure data were obtained in lab analysis from oilfield K in Serbia. From the Leverett  $J$  function ( $S_w$ ) for changed values of porosity ( $\phi$ ) and permeability ( $K$ ) change in capillary pressure, ( $P_c$ ) was recalculated for all three cases. Capillary pressure data for all cases are shown in Table 4, where  $S_w$  is water saturation,  $P_c$  is capillary pressure and  $J(S_w)$  is Leverett  $J$  function.

**Table 4.** Capillary pressure data for all cases.

Reservoir		Case I		Case II		Case III		
$S_w$	$P_c$ (bar)	$J(S_w)$	$J(S_w)$	$P_c$ (bar)	$J(S_w)$	$P_c$ (bar)	$J(S_w)$	$P_c$ (bar)
0.24	10.0869	12.2830	8.8115	7.2830	7.8656	6.5012	7.5493	6.2398
0.25	7.1809	8.7443	6.2730	5.1848	5.5996	4.6282	5.3744	4.4421
0.3	4.2000	5.1144	3.6689	3.0325	3.2751	2.7070	3.1434	2.5981
0.35	2.7000	3.2878	2.3586	1.9495	2.1054	1.7402	2.0208	1.6702
0.4	1.8200	2.2162	1.5899	1.3141	1.4192	1.1730	1.3621	1.1259
0.45	1.4500	1.7657	1.2667	1.0469	1.1307	0.9346	1.0852	0.8970
0.5	1.1914	1.4508	1.0408	0.8602	0.9290	0.7679	0.8917	0.7370
0.55	1.0200	1.2421	0.8910	0.7365	0.7954	0.6574	0.7634	0.6310
0.6	0.8500	1.0351	0.7425	0.6137	0.6628	0.5478	0.6362	0.5258
0.65	0.7300	0.8889	0.6377	0.5271	0.5692	0.4705	0.5464	0.4516
0.7	0.6000	0.7306	0.5241	0.4332	0.4679	0.3867	0.4491	0.3712
0.8	0.4600	0.5601	0.4018	0.3321	0.3587	0.2965	0.3443	0.2846
0.91	0.3532	0.4301	0.3086	0.2550	0.2754	0.2277	0.2644	0.2185

Changes in capillary pressure are shown in Figure 5.

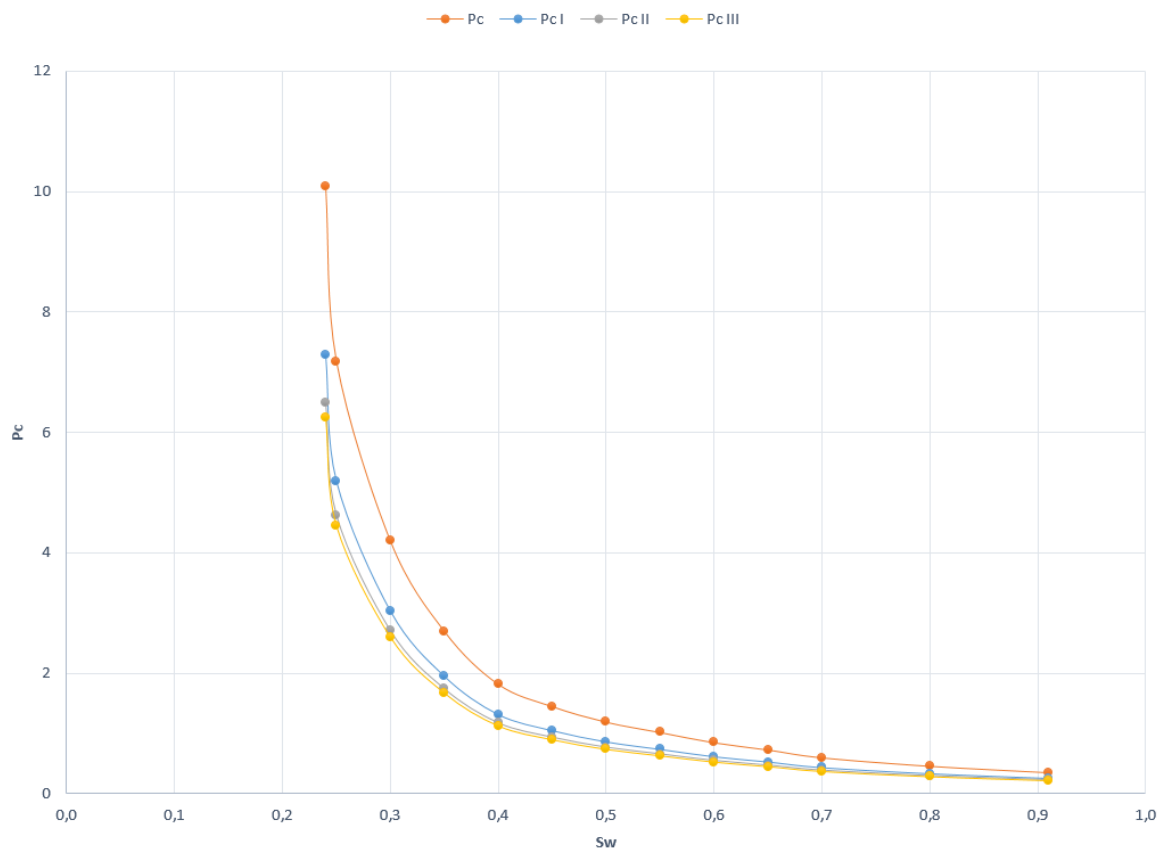


**Figure 5.** Changes in capillary pressure.

#### 4.4. Changes of Relative Permeabilities

From capillary pressure data, relative permeabilities were calculated for oil and water using the modified Brooks and Corey correlations with the rock quality index ratio. The rock quality index ratio for all three cases is shown in Table 5.

**Table 5.** Calculated rock quality index ratio for all three cases.

	RQI	R <sub>RQI</sub>
Reservoir	42.35	1
Case I	30.57	1.38
Case II	27.29	1.55
Case III	26.20	1.62

Changes in relative permeability are shown in Figure 6.

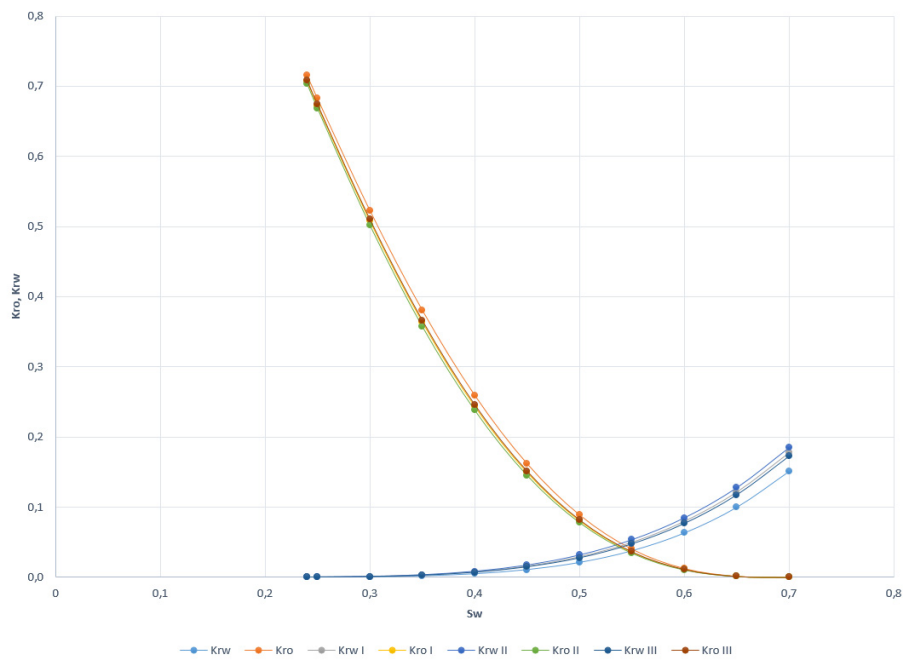


Figure 6. Calculated changes of relative permeabilities.

#### 4.5. Effects on Oil Displacement

Buckley–Leverett curve of oil displacement is shown in Figure 7.

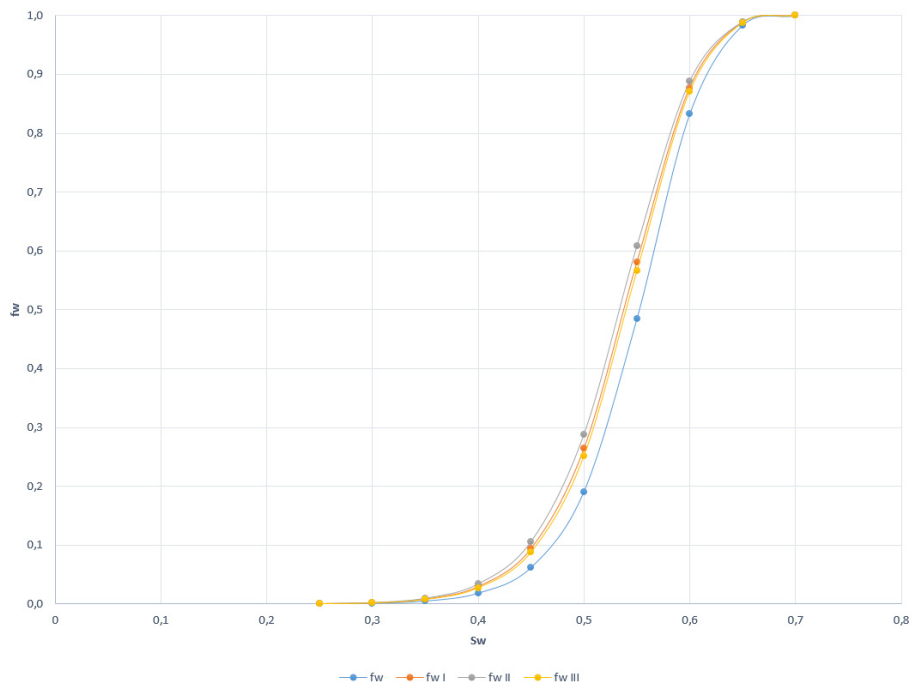


Figure 7. Calculated Buckley–Leverett curve of oil displacement.

### 5. Discussion

This model is based on the theory of suspended solids deposition and entrainment in porous media developed by Gruesbeck and Collins, and Tod et al. [17,18]. Three types of water with different suspended solids distributions were analyzed. In Case I, where injection water contains small-range

diameters of suspended solids, calculated porosity reduction was 2.95% (from 18.7% to 15.75%), while permeability decreased 188.13 mD (from 335.32 to 147.19 mD). In Case II, where injection water contained mid-range diameters of suspended solids, calculated porosity reduction was 3.87% (from 18.7% to 14.83%), while permeability decreased 224.86 mD (from 335.32 to 110.46 mD). In Case III, where injection water contained large-range diameters of suspended solids, calculated porosity reduction was 4.18% (from 18.7% to 14.52%), while permeability decreased 235.75 mD (from 335.32 to 99.57 mD). Decreases in porosity and permeability were observed in all three cases, which were confirmed in the experimental study by Tod et al. [18] and Oort et al. [21]. In Case III, it could be concluded that there was an external filter cake. After calculating the porosity and permeability decreases, changes in capillary pressure were calculated using the Leverett J function. Results obtained from the modified Brooks and Corey relative permeability model showed a slight decrease in relative permeability for oil and an increase in relative permeability for water in all three cases. It can be explained as a mutual effect of changing reservoir properties due to pore-clogging from suspended solids. The presented model showed a greater impact on permeability reduction that was expected with an injection of water with suspended solids due to the pore clogging and formation impairment. Waters I, II, and III had a similar effect on oil displacement affecting the displacement efficiency. With pore clogging and formation impairment, a specific volume of oil would not be displacement effectively.

## 6. Conclusions

In this paper, an analytical model for predicting the effects of suspended solids on oil displacement during waterflooding operations was presented. The presented analytical model showed the influence of suspended solids in injection water on oil displacement during waterflooding operations. Formation impairment was present in every case, regardless of suspended solids diameter, and results showed that formation damage occurred even with small particles that were confirmed in previous experimental studies on core samples. Suspended solids have the greatest influence on porosity and permeability impairment. Furthermore, formation impairment affects relative permeability and oil displacement in all three cases.

This model can be used as an input for reservoir modelling studies for monitoring and controlling displacement efficiency during waterflooding. It is possible to adapt filtration units to enhance water injectivity and prevent formation damage caused by suspended solids. Suspended solids quantity can be reduced with filtration or cyclone treatment; however, the cost of treatment could be compared with alternative methods, such as periodic acid stimulations of injection wells and the presented model could be used for this decision. Water quality is not a static parameter, and suspended solids distribution is a parameter under constant changes. This methodology needs to be applied periodically to check injected water quality on reservoir impairment and displacement efficiency.

**Author Contributions:** Conceptualization, S.N., V.M.; Methodology, S.N., V.M.; Software, S.N., V.M., D.G.; Formal analysis, S.N., V.M., A.Z., D.G.; Resources, S.N.; Writing—original draft preparation, S.N., D.G.; Writing—review and editing, S.N., A.Z., A.D.; Supervision, A.Z., A.D. All authors have read and agreed to the published version of the manuscript.

**Funding:** This research received no external funding.

**Conflicts of Interest:** The authors declare no conflict of interest.

## References

1. Davarpanah, A.; Mirshekari, B.; Razmjoo, A.A. A Simulation Study of Water Injection and Gas Injectivity Scenarios in a Fractured Carbonate Reservoir: A Comparative Study. *Pet. Res.* **2019**, *4*, 250–256. [[CrossRef](#)]
2. Davarpanah, A.; Mirshekari, B. Mathematical Modeling of Injectivity Damage with Oil Droplets in the Waste Produced Water Re-Injection of the Linear Flow. *Eur. Phys. J. Plus* **2019**, *134*, 180. [[CrossRef](#)]
3. Afshin, D. Feasible Analysis of Reusing Flowback Produced Water in the Operational Performances of Oil Reservoirs. *Environ. Sci. Pollut. Res.* **2018**, *25*, 35387–35395.

4. Davarpanah, A.; Mirshekari, B.; Jafari Behbahani, T.J.; Hemmati, M. Integrated production logging tools approach for convenient experimental individual layer permeability measurements in a multi-layered fractured reservoir. *J. Petrol. Explor. Prod. Technol.* **2018**, *8*, 743–751. [[CrossRef](#)]
5. Costier, L.; van den Hoek, P.J.; Davidson, C.J.; Ding, M.; van den Berg, J.T.; Hofland, R. Establishing Water Injection Dynamics by Leading-Edge Coreflood Testing. In Proceedings of the EUROPEC/EAGE Conference and Exhibition, Amsterdam, The Netherlands, 8–11 June 2009. [[CrossRef](#)]
6. Davarpanah, A.; Mirshekari, B. Experimental Investigation and Mathematical Modeling of Gas Diffusivity by Carbon Dioxide and Methane Kinetic Adsorption. *Ind. Eng. Chem. Res.* **2019**, *58*, 12392–12400. [[CrossRef](#)]
7. Faruk, C. Formation Damage Mechanisms and Their Phenomenological Modeling—An Overview. In Proceedings of the European Formation Damage Conference, Scheveningen, The Netherlands, 30 May–1 June 2007. [[CrossRef](#)]
8. Hussain, F.; Zeinjahromi, A.; Bedrikovetsky, P.; Badalyan, A.; Carageorgos, T.; Cinar, Y. An Experimental Study of Improved Oil Recovery through Fines-Assisted Waterflooding. *J. Pet. Sci. Eng.* **2013**, *109*, 187–197. [[CrossRef](#)]
9. Faruk, C. *Reservoir Formation Damage: Fundamentals, Modeling, Assessment, and Mitigation*; Elsevier: Amsterdam, The Netherlands; Gulf Professional Publishing: Amsterdam, The Netherlands, 2016.
10. Hofsaess, T.; Kleinitz, W. 30 Years of Predicting Injectivity after Barkman & Davidson: Where Are We Today? In Proceedings of the SPE European Formation Damage Conference, The Hague, The Netherlands, 13–14 May 2003. [[CrossRef](#)]
11. Vaz, A.S.L.; Pavel, G. Bedrikovetsky, Claudio Jose Alves Furtado, Alexandre Guedes Siqueira, and Antonio Luiz Serra De Souza. In Effects of Residual Oil on Re-Injection of Produced Water. In Proceedings of the SPE Europec/EAGE Annual Conference and Exhibition, Vienna, Austria, 12–15 June 2006. [[CrossRef](#)]
12. Buret, S.; Nabzar, L.; Jada, A. Water Quality & Well Injectivity: Do Residual Stable Oil-in-Water Emulsions Matter? In Proceedings of the 8th European Formation Damage Conference, Scheveningen, The Netherlands, 27–29 May 2009.
13. Khatib, Z.I. Prediction of Formation Damage Due to Suspended Solids: Modeling Approach of Filter Cake Buildup in Injectors. In Proceedings of the SPE Annual Technical Conference and Exhibition, New Orleans, LA, USA, 25–28 September 1994. [[CrossRef](#)]
14. Pang, S.; Sharma, M.M. A Model for Predicting Injectivity Decline in Water-Injection Wells. *SPE Form. Eval.* **1997**, *12*, 194–201. [[CrossRef](#)]
15. Bedrikovetsky, P.; Marchesin, D.; Shecaira, F.; Souza, A.I.; Milanez, P.V.; Rezende, E. Characterisation of Deep Bed Filtration System from Laboratory Pressure Drop Measurements. *J. Pet. Sci. Eng.* **2001**, *32*, 167–177. [[CrossRef](#)]
16. Shedid, E. A Novel Technique for the Determination of Microscopic Pore Size Distribution of Heterogeneous Reservoir Rocks. In Proceedings of the Asia Pacific Oil and Gas Conference and Exhibition, Jakarta, Indonesia, 30 October–1 November 2007.
17. Gruesbeck, C.; Collins, R.E. Entrainment and Deposition of Fine Particles in Porous Media. *Soc. Pet. Eng. J.* **1982**, *22*, 847–856. [[CrossRef](#)]
18. Todd, A.C.; Somerville, J.E.; Scott, G. The Application of Depth of Formation Damage Measurements in Predicting Water Injectivity Decline. In Proceedings of the SPE Formation Damage Control Symposium, Bakersfield, CA, USA, 13–14 February 1984. [[CrossRef](#)]
19. Davidson, D.H. Invasion and Impairment of Formations by Particulates. In Proceedings of the SPE Annual Technical Conference and Exhibition, Las Vegas, NV, USA, 23–26 September 1979. [[CrossRef](#)]
20. Vitthal, S.; Sharma, M.M.; Sepehrnoori, K. A One-Dimensional Formation Damage Simulator for Damage Due to Fines Migration. In Proceedings of the SPE Formation Damage Control Symposium, Bakersfield, CA, USA, 8–9 February 1988. [[CrossRef](#)]
21. Van Oort, E.; Van Velzen, J.F.; Leerlooijer, K. Impairment by Suspended Solids Invasion: Testing and Prediction. *SPE Prod. Facil.* **1993**, *8*, 178–184. [[CrossRef](#)]
22. Hutchinson, C.A. Effect of Data Errors on Typical Reservoir Engineering Calculations. In Proceedings of the Fall Meeting of the Petroleum Branch of AIME, Oklahoma City, OK, USA, 3–5 October 1951. [[CrossRef](#)]
23. Ling, K.; Han, G.; Shen, Z.; Ghalambor, A.; He, J.; Pei, P. Calculating Pore Size Distribution by Using Capillary Pressure. In Proceedings of the SPE International Symposium and Exhibition on Formation Damage Control, Lafayette, LA, USA, 26–28 February 2014. [[CrossRef](#)]

24. Burdine, N.T.; Gournay, L.S.; Reichertz, P.P. Pore Size Distribution of Petroleum Reservoir Rocks. *J. Pet. Technol.* **1950**, *2*, 195–204. [[CrossRef](#)]
25. Klinkenberg, L.J. Pore Size Distribution of Porous Media and Displacement Experiments with Miscible Liquids. *J. Pet. Technol.* **1957**, *9*, 63–66. [[CrossRef](#)]
26. Pickell, J.J.; Swanson, B.F.; Hickman, W.B. Application of Air-Mercury and Oil-Air Capillary Pressure Data in the Study of Pore Structure and Fluid Distribution. *Soc. Pet. Eng. J.* **1966**, *6*, 55–61. [[CrossRef](#)]
27. Dullien, F.A.L. Determination of Pore Accessibilities—An Approach. *J. Pet. Technol.* **1969**, *21*, 14–15. [[CrossRef](#)]
28. Pandey, B.P.; Singhal, A.K. Evaluation of the Capillary Pressure Curve Techniques for Determining Pore Size Distribution—A Network Approach. *Powder Technol.* **1976**, *15*, 89–96. [[CrossRef](#)]
29. Yuan, H.H.; Swanson, B.F. Resolving Pore-Space Characteristics by Rate-Controlled Porosimetry. *SPE Form. Eval.* **1989**, *4*, 17–24. [[CrossRef](#)]
30. Tomutsa, L.; Mahmood, S.M.; Brinkmeyer, A.; Honarpour, M. Application of Integrated Pore-to-Core Image Analysis to Study Fluid Distribution in Reservoir Rocks. In Proceedings of the SPE Annual Technical Conference and Exhibition, New Orleans, LA, USA, 23–26 September 1990.
31. Bijan, B. Quantitative Characterization of Carbonate Pore Systems by Mercury- Injection Method and Image Analysis in a Homogeneous Reservoir. In Proceedings of the Middle East Oil Show, Manama, Bahrain, 9–12 June 2003. [[CrossRef](#)]
32. Homgxue, H.; Maurice, B.; Ioannidis, M.; Xu, B. Multiscale Pore Structure Characterization by Combining Image Analysis and Mercury Porosimetry. In Proceedings of the SPE Europec/EAGE Annual Conference and Exhibition, Vienna, Austria, 12–15 June 2006.
33. Ghazanfari, M.H.; Rashtchian, D.; Kharrat, R.; Vossoughi, S. Capillary Pressure Estimation Using Statistical Pore Size Functions. *Chem. Eng. Technol.* **2007**, *30*, 862–869. [[CrossRef](#)]
34. Dong, H.; Touati, M.; Blunt, M.J. Pore Network Modeling: Analysis of Pore Size Distribution of Arabian Core Samples. In Proceedings of the SPE Middle East Oil and Gas Show and Conference, Manama, Bahrain, 11–14 March 2007.
35. Martin, C.A.; Ramia, M.; Barberis, L. The Centrifuge as a Tool to Determine the Pore-Throat Size Distribution in Plugs. In Proceedings of the Latin American & Caribbean Petroleum Engineering Conference, Buenos Aires, Argentina, 15–18 April 2007.
36. Kegang, L. Correlation between Rock Permeability and Formation Resistivity Factor—A Rigorous and Theoretical Derivation. In Proceedings of the SPE Middle East Unconventional Gas Conference and Exhibition, Abu Dhabi, UAE, 23–25 January 2012.
37. Izadi, M.; Ghalambor, A. A New Approach in Permeability and Hydraulic Flow Unit Determination. In Proceedings of the SPE International Symposium and Exhibition on Formation Damage Control, Lafayette, LA, USA, 15–17 February 2012. [[CrossRef](#)]
38. Mumuni, A.; Miadonye, A. The Accuracy of Pore Size Distribution Index Using Capillary Pressure Data: Effect of Physiochemical Factors. *J. Hydrogeol. Hydrol. Eng.* **2018**, *6*. [[CrossRef](#)]
39. Anovitz, L.M.; Cole, D.R. Characterization and Analysis of Porosity and Pore Structures. *Rev. Mineral. Geochem.* **2015**, *80*, 61–164. [[CrossRef](#)]
40. Main, G.V. Chilingar Richard. Relationship between Porosity, Permeability, and Surface Areas of Sediments. *SEPM J. Sediment. Res.* **1963**, *33*, 759–765. [[CrossRef](#)]
41. Chilingar, G.V. Relationship between Porosity, Permeability, and Grain-Size Distribution of Sands and Sandstones. *Dev. Sedimentol. Deltaic Shallow Mar. Depos.* **1964**, 71–75. [[CrossRef](#)]
42. Antonio, C. Permeability-Porosity Relationship: A Reexamination of the Kozeny-Carman Equation Based on a Fractal Pore-Space Geometry Assumption. *Geophys. Res. Lett.* **2006**, *33*. [[CrossRef](#)]
43. Kotyakhov, F.I. Interrelationship between major physical parameters of sandstones. *Neft Khas* **1949**, *12*, 29–32.
44. Adler, P.; Jacquin, C.; Quiblier, J. Flow in simulated porous media. *Int. J. Multiph. Flow* **1990**, *16*, 691–712. [[CrossRef](#)]
45. Zhang, S.; Lu, P.; Cantrell, D.; Zaretskiy, Y.; Jobe, D.; Agar, S.M. Improved Quantification of the Porosity–Permeability Relationship of Limestones Using Petrographical Texture. *Pet. Geosci.* **2017**, *24*, 440–448. [[CrossRef](#)]
46. Lucia, F.J. Rock-Fabric, Petrophysical Parameters, and Classification. *Carbonate Reserv. Charact.* **1999**, 23–57. [[CrossRef](#)]

47. Nelson, H.P. Permeability-porosity Relationships in Sedimentary Rocks. Society of Petrophysicists & Well Log Analysts. *Log Anal.* **1994**, *35*, 38–62.
48. Leverett, M.C.; Lewis, W.B. Steady Flow of Gas-Oil-Water Mixtures through Unconsolidated Sands. *Trans. AIME* **1941**, *142*, 107–116. [[CrossRef](#)]
49. Al-Ajmi, F.A.; Holditch, S.A. Permeability Estimation Using Hydraulic Flow Units in a Central Arabia Reservoir. In Proceedings of the SPE Annual Technical Conference and Exhibition, Dallas, TX, USA, 1–4 October 2000.
50. Brooks, R.H.; Corey, A.T. Properties of porous media affecting fluid flow. *J. Irrig. Drain. Div.* **1966**, *92*, 61–90.
51. Buckley, S.E.; Leverett, M.C. Mechanism of Fluid Displacement in Sands. *Trans. AIME* **1942**, *146*, 107–116. [[CrossRef](#)]



© 2020 by the authors. Licensee MDPI, Basel, Switzerland. This article is an open access article distributed under the terms and conditions of the Creative Commons Attribution (CC BY) license (<http://creativecommons.org/licenses/by/4.0/>).